Cambridge Default Journal (2023), **XX**, 1–30

CAMBRIDGE
UNIVERSITY PRESS

ARTICLE TYPE

Future insurance losses for pluvial flooding in Canada and the United States

Mathilde Bourget,[†] Mathieu Boudreault,[*‡] David A. Carozza,[‡] Jérémie Boudreault,[¶] and Sébastien Raymond[¶]

†Department of Mathematics, Université du Québec à Montréal, Montréal, QC, Canada and Collège Jean-de-Brébeuf, Montréal, QC, Canada
‡Department of Mathematics, Université du Québec à Montréal, Montréal, QC, Canada
¶Climatic Hazards and Advanced Risk Modelling, Co-operators General Insurance Company, Québec, QC, Canada and Centre Eau Terre Environnement, Institut national de la recherche scientifique, Québec, QC, Canada
*Corresponding author. Email: boudreault.mathieu@uqam.ca

Abstract

There is mounting pressure on the financial services industry to factor in climate extremes and climate change. As a result, new reporting and regulatory requirements are gradually being enforced on (re)insurers globally. One key requirement is physical risk assessment, that is, quantifying the financial impacts of climate change on the frequency and severity of claims due to weather events such as flooding. This is however a very challenging task for (re)insurers as it requires modelling at the scale of a portfolio and at a high enough spatial resolution to incorporate local climate change effects.

In this paper, we introduce a data science approach to physical risk assessment of pluvial flooding for insurance portfolios over Canada and the United States. The underlying flood model is focused on quantifying the financial impacts of short-term (12–48 hours) precipitation dynamics over the present (2010–2030) and future climate (2040–2060) using a methodological approach that leverages statistical/machine learning and regional climate models. The flood model is designed for applications that do not require street-level precision as is often the case for scenario and trend analyses. It is performed at the full scale of Canada and the U.S. at 10 to 25 km resolution.

Our models show that climate change and urbanization will typically increase losses over Canada and the U.S., while impacts are strongly heterogeneous from one state or province to another, or even within a territory. Portfolio applications highlight the importance for a (re)insurer to differentiate between future changes in hazard and exposure, as the latter may magnify or attenuate the impacts of climate change on losses. While the overall methodology can be applied to physical risk assessment of various risks, we also provide detailed maps and tables of the impacts of climate change on pluvial flooding for use by researchers and practitioners.

Keywords: flood insurance, pluvial flooding, climate change, physical risk assessment, machine/statistical learning, climate models

1. Introduction

Flooding is the most significant natural hazard in the United States and Canada (FEMA 2017; Canada 2022b). With estimated average annual losses of about $20B (USD) in the United States (FSF 2021) and of $3B (CAD) in Canada (PSC 2022), flooding represents a significant threat to many urban, rural and coastal communities. Availability of insurance or financial assistance, from either public or private programs, is therefore very important to increase the resilience of these vulnerable communities (Surminski, Bouwer, and Linnerooth-Bayer 2016; Kousky 2022).

Access to insurance (or financial assistance) and adaptation strategies however largely differ for fluvial, pluvial and coastal flooding. For example, basement flooding whose root cause is the overflow of a river is typically covered by public plans whereas sewer backup is not (FEMA 2005). It is therefore imperative for actuaries, economists, land planners, policy- and decision-makers to distinguish the underlying causes of flooding. Fluvial or riverine flooding refers to the overflow of a river or watercourse; pluvial flooding refers to "heavy rainfall-related flooding that is independent of an overflowing body of water" (ICLR 2021) which includes flash floods, whereas coastal flooding refers to flooding of the coastlines due for example to storm surge (one can find similar definitions in IBC 2015; Mitchell-Wallace et al. 2017; ICLR 2021; FEMA 2023).

Climate change should affect each type of flooding very differently. According to the Intergovernmental Panel on Climate Change (IPCC) 6th Assessment Report (IPCC 2022), there is high confidence of an increase of heavy precipitation and pluvial flooding in Canada and the U.S. with the exception of the Northern West Coast of the U.S. that has medium confidence. As for river flooding, there appears to be a medium confidence of an increase over both the U.S. and Canada. The complex interactions between temperature rise, snowmelt and heavy short-term precipitation (over 24-48 hours) dynamics, make it difficult to detect an increasing or decreasing trend in fluvial flooding in various parts of Canada and the U.S. (Bush and Lemmen 2019), especially over the winter and spring. This further reinforces the idea of differentiating the types of flooding for financial risk management.

There is currently pressure on the financial services industry to factor in climate extremes and climate change in their business decisions. This is because corporations globally are integrating ESG principles (environmental, social, and corporate governance), and will soon become subject to a new regulatory environment, thanks in large part to the work of the Task Force on Climate-related Financial Disclosures (TCFD) (Financial Stability Board 2017). Regulators are gradually requiring corporations to report the sensitivity of their profitability to various scenarios of climate change whereas banks and (re)insurers must do similarly by stress-testing their stability as well (e.g., Bank of England 2019; OSFI 2023).

An important component of such reporting and stress-testing for the property (re)insurance industry is physical risk assessment (PRA); that is, quantifying the financial impact of climate change on the frequency and intensity of claims due to e.g., flooding. The ability to distinguish regions of Canada and the U.S. where climate change might have the most (or least) impact is obviously critical for PRA. For example, Environment and Climate Change Canada found that temperature increase in Canada is expected to be steeper than elsewhere, especially in Northern territories (Bush and Lemmen 2019; IPCC 2022). Evidence for more frequent and more severe atmospheric rivers is also mounting (Gershunov et al. 2019; Corringham et al. 2019; Rhoades et al. 2020) as British Columbia and California struggled with record amounts of rain and flooding in 2021 and 2022. Sound decision-making thus requires modelling of the financial impacts of climate change at the scale of a (re)insurance portfolio and at a spatial resolution that allows the integration of local climate change effects.

There are however important limitations to meet these objectives. Large scale high-resolution flood modeling is (1) extremely costly from both a computational and financial standpoint; (2) they require inputs that are difficult to acquire for large countries (high-resolution terrain and bathymetry data) or are non-existent for many cities (sewer system configuration, exact location of inlets and outlets) and ultimately; (3) they lack the flexibility required by e.g., actuaries and economists to analyze many customized scenarios (for a review, see Carozza and Boudreault 2021 and references therein). Computing the impacts of climate change on flooding adds another layer of difficulty with respect to modelling future temperature and precipitation dynamics. This requires integration of climate models whose outputs are limited at the global scale because they must be run on large computer clusters. For financial risk management applications that do not necessarily require accurate

street-level data, such as analyzing many different scenarios and trends for (re)insurance portfolios over Canada and/or the U.S., the resolution provided by climate models is appropriate.

In this paper, we introduce a data science approach to physical risk assessment of pluvial flooding for insurance portfolios over Canada and the U.S. That is, the underlying flood model is focused on quantifying the financial impacts of short-term (12–48 hours) precipitation dynamics over the present and future climate (until 2060) using a methodological approach that leverages statistical/machine learning and climate models. This is done through a top-down modelling chain integrating climate model outputs at its core. Few papers in actuarial science have integrated climate models for insurance applications. For example Boudreault et al. 2020 used a top-down modelling approach, and a chain of climate, hydrological and hydraulic models to represent fluvial flood risk over a small city in Canada. Jin and Erhardt 2020 used climate model outputs to price temperature index–based insurance products in California. Here, the analysis is performed for Canada and the U.S. at 10 or 25 km resolution depending on the application, keeping an appropriate balance between computational speed and the ability to distinguish regional discrepancies.

To meet such goal, we trained statistical and machine learning methods on historical pluvial flood occurrences in the United States, and validated their predictive skill over the U.S. (test set) and Canada (validation set). We then integrated output from a regional climate model to calculate future flood probabilities for every month and grid cell until 2060. Finally we show various portfolio applications where we analyze the impacts of changes in hazard and exposure on portfolio losses over the present (2010–2030) and future (2040–2060). The paper provides a methodological framework for physical risk assessment that is applicable to various risks, connecting statistical and climate models to solve a problem that is increasingly important for both actuarial science and actuaries. To the best of our knowledge, this is the first paper that provides a financial assessment of the impacts of climate change on pluvial flooding over Canada and the U.S. for insurance purposes.

Overall, we find that Generalized Additive Models have a solid predictive power in- and out-of-sample to explain pluvial flood episodes compared to linear models and ensemble tree-based methods. We thus find different levels of pluvial flood risk in most urban areas of Canada and the U.S. Furthermore, we do not recommend using tree-based methods for projecting the impacts of future precipitation and urbanization patterns due to their inability to extrapolate beyond the original training set. There also appears to be wide heterogeneity of climate change impacts across states and provinces that become significant when analyzing insurance portfolios, highlighting the importance of climate-informed financial risk management. We also emphasize the importance of differentiating changes in hazard and exposure since they both interact to attenuate or magnify the financial impacts of climate change.

The paper is structured as follows. Section 2 describes the general physical risk assessment framework and how it is applied in the context of this paper. Section 3 then details the datasets, statistical and machine learning methods used to build the various pluvial flood models discussed in the paper. Evaluation of the predictive power of the models over test and validation sets is also presented in this section. We then show future projections of pluvial flood risk in Section 4 by first describing the data, methods and validations. We provide maps over Canada and the United States of the impacts of climate change on pluvial flooding as well as time series for pluvial flood probabilities for select cities in both countries. We present a portfolio application in Section 5 highlighting how regional discrepancies and portfolio composition may affect aggregate losses. Section 6 then concludes with a broad discussion of the paper's findings. Appendices and the Supplementary Material complete the core analyses of the paper by providing additional results and validations.

2. Physical risk assessment

Physical climate risk assessment or physical risk assessment (PRA) in the context of this paper is the qualitative and quantitative analysis of the impacts of climatic events such as floods, tropical

cyclones, wildfires, etc. For a property and casualty insurance organization (public or private), PRA requires an understanding of the frequency and intensity of these events, without or with climate change considerations, and their impact on the claims dynamics. This is typically done through a decomposition of risk into its main components, that is, hazard, vulnerability and exposure (Mitchell-Wallace et al. 2017). This section describes general principles of PRA and how we approach the latter to evaluate portfolio losses from pluvial flooding under the present and future climates.

2.1 Top-down catastrophe modelling

According to the United Nations Office for Disaster Risk Reduction (UNDRR) Sendai Framework Terminology on Disaster Risk Reduction (UNDRR 2017), hazard, vulnerability and exposure are defined as (IPCC 2021a uses a similar terminology):

- "Hazard: a process, phenomenon or human activity that may cause loss of life, injury or other health impacts, property damage, social and economic disruption or environmental degradation;
- Vulnerability: the conditions determined by physical, social, economic and environmental factors or processes which increase the susceptibility of an individual, a community, assets or systems to the impacts of hazards;
- Exposure: the situation of people, infrastructure, housing, production capacities and other tangible human assets located in hazard-prone areas."

Risk is the intersection of hazard, vulnerability and exposure: for a visual depiction of risk as a function of hazard, vulnerability and exposure, one should look at Figure 1 of UN 2023 or Figure TS.4 of IPCC 2021b. For example, a property is exposed to flooding if it is located in an area of flood hazard, whereas it is vulnerable to flooding if there are possible entries where water can enter into a house (basement windows, doors). Catastrophe modelling is therefore naturally based upon such decomposition of risk and aims to model each of these three components, providing in the end what is known as the ground-up loss, that is losses before the application of any insurance or reinsurance. This is illustrated at the bottom of Figure 1.

The hazard component represents the frequency, intensity, duration, genesis location and footprint of an event. The exposure includes the geographical location of the property, its size (e.g., square footage, number of floors) and value (e.g., market value, reconstruction costs). Vulnerability represents the characteristics of a house that magnify or attenuate the impacts of the hazard. In the context of flooding, that includes whether there is a finished basement or not or a crawlspace, first floor elevation, height of basement windows, etc. Damage curves typically link the intensity of an hazard with the vulnerability of a home to yield dollars of losses or percentage of damage.

2.2 Climate models

Hazard modelling of climatic events such as flooding or tropical cyclones is founded on an understanding of the interactions between the climate and e.g., the frequency and intensity of a climatic hazard as illustrated at the top of Figure 1. PRA under future climates adds another layer of modelling as we need to relate greenhouse gas (GHG) emissions and concentration to impacts on e.g., temperature and precipitation. A natural approach is therefore the integration of climate models (general circulation models and regional climate models) into a PRA.

General circulation models (GCMs) are numerical models that simulate the evolution and interactions of most components of the climate system (atmosphere, land, ocean, ice, etc.) using physical equations and empirical relationships (Chen et al. 2021). They are at the core of climate and climate change studies and are thus widely used to study global temperature and precipitation (among other variables) patterns over the present and future (Chen et al. 2021). In many respects regional climate models (RCMs) are similar to GCMs yet they usually focus on atmospheric phenomena at continental and regional scales allowing for simulations that use higher spatial and temporal resolutions

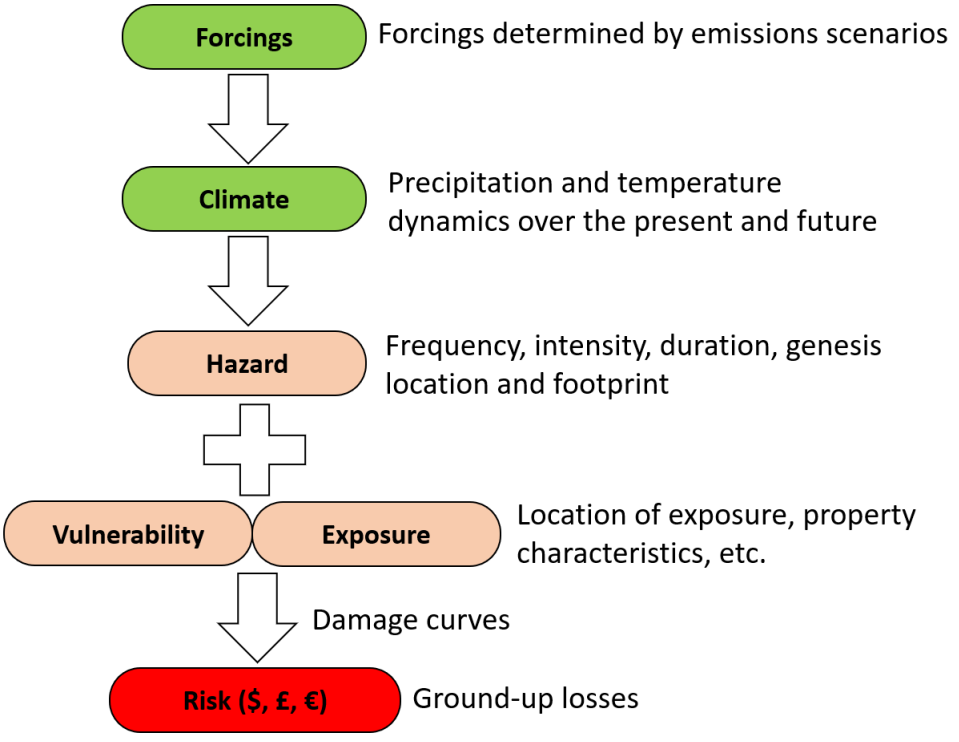

Figure 1. Top-down catastrophe modelling approach with climate on top

and are able to resolve smaller-scale processes (Chen et al. 2021). Climate models are therefore computationally intensive and are typically run on supercomputers.

Climate models are forced with GHG emissions scenarios that are designed to capture the impacts of future socioeconomic growth and energy choices. Those emissions scenarios are in turn converted into radiative forcings (see top of Figure 1). Changes in the radiative forcing represent the extra heat in the atmosphere due to GHG emissions and are measured in watts per squared-meter. For example, in the IPCC AR6, the climate scenario SSP2-4.5 represents what is known as the "middle of the road" (the entire storyline is provided in Fricko et al. 2017) and corresponds to $4.5 Wm^{-2}$ of extra energy flux to the atmosphere by 2100. Over available climate models, this emissions scenario typically leads to an approximate global warming of +2.5 degrees in 2100 compared to pre-industrial.

Typical outputs of climate models include (surface) temperature, precipitation (liquid, convective, snow, etc.), near surface relative/specific humidity, Eastward/Northward (near surface) winds, (surface) air pressure, etc. Outputs typically are stored as grids and may take up to terabytes and petabytes of storage depending on the vertical (in the atmosphere), horizontal (over the surface) and temporal (hourly, daily) resolution of the data, the variables needed, etc.

Integrating climate models into hazard modelling should also take into consideration the biases in the outputs that can affect the results at the end of the modelling chain. This is typically approached using what is called pre-processing or post-processing. Pre-processing implies bias correction prior to using it into a hazard module. This is done by comparing e.g., the precipitation outputs with past observations. Post-processing implies comparing a hazard feature simulated from climate model outputs (for example hazard frequency) with what was observed in the past. If pre-processing does not succeed in eliminating all biases in the hazard component, then post-processing would also be needed.

Reporting and regulatory requirements are often based upon assessing the overall impacts on the organization of a given temperature increase (say e.g., +2 degrees compared to pre-industrial). Temperature increase and global warming are endogenous in a climate model and result from radiative forcings. Integrating climate models into PRA therefore requires using available runs of climate models along with corresponding climate scenarios.

2.3 Proposed approach

In this paper, we take a data science approach to PRA of pluvial flooding in an insurance portfolio. The core of the work lies in the hazard modelling of pluvial flooding occurrence (Y) as a function of a set of atmospheric and socioeconomic variables (X). We first fit and validate the $Y|X$ relationship using statistical and machine learning for binary responses using past observed data for X and Y. This is the fitting and validation step. Then climate risk assessment is performed by computing flood occurrence probabilities using outputs from climate models for X over different time intervals. This is the projection and simulation step. When computing predictions, one may hold fixed socioeconomic variables to isolate the effects of climate change from socioeconomic growth or one may use population projections as well.

This study is not meant to provide a detailed account of the impacts of pluvial flooding at the street-level. There is inevitably a trade-off between the financial and/or computing resources necessary and the resolution of the information needed. Here, we focus on the large-scale impacts of climate change on pluvial flooding in portfolios covering either Canada or the United States. As such, we do not explicitly model vulnerability while we proxy exposure as the number of people living or insured in each grid cell. More details about portfolio modelling are provided in Section 5.

3. Occurrence Models

This section describes the pluvial flood occurrence models analyzed throughout the paper. We begin by outlining the datasets (Section 3.1), the statistical and machine learning methods (Section 3.2), then we explain how they have been applied to our study (Section 3.3) and finish the section by assessing the predictive capability of the models in the United States and Canada (Sections 3.4.1 and 3.4.2).

3.1 Data

This section characterizes the historical flood occurrence data (Section 3.1.1) used as the response variable in the statistical and machine learning models. Then we examine the predictors made from atmospheric and socioeconomic variables (Sections 3.1.2 and 3.1.3).

3.1.1 Flood occurrence

Historical flood occurrence is derived from the Storm Events Database (SED) from the National Oceanic and Atmospheric Administration (NOAA) (NOAA 2021). The dataset contains significant weather events from 1951 and onward in the United States (no similar dataset is available for Canada and this is discussed in Section 3.4.2). Information comes from multiple sources, that is, 911 call centers, media, and local authorities (such as law enforcement). For each event, there are many variables available, that is, the date and time of the beginning and end of the event, the location of the event, type of event and for flooding events, the cause of such flooding. For the purpose of this research, we focused on flooding events induced by heavy rain between 2007 and 2020 because latitude/longitude location data was not available prior to 2007.

We then converted the storm events location data into monthly grid cells over the United States, so there is at most one event per grid cell-month. We chose a monthly observation frequency to capture seasonality while keeping the overall size of the dataset manageable. We fixed the grid

cell resolution to $0.1° \times 0.1°$ to match precipitation data (Section 3.1.2). Such spatial resolution is approximately equivalent to 10 km $\times$10 km over the area of study (but as we approach the North Pole, the grid cell area expressed in km^2 decreases). Therefore, historical flood occurrence data (and covariates as well) is represented over 168 grids (1 per month over 14 years) of 143,922 cells each.

3.1.2 Atmospheric variables

Precipitation is obviously a key driver of pluvial flooding and data is extracted from the Multi-Source Weighted-Ensemble Precipitation (MSWEP), a comprehensive dataset that combines rain gauges, satellites and reanalyses from various sources (Beck et al. 2019). The 3-hourly data is available globally at a spatial resolution of $0.1° \times 0.1°$ from 1979 and onward but we extracted data from 2007 to 2020 to match the flood occurrence data. We built precipitation covariates by computing the monthly maximum of 6-, 9-, 12-, 24- and 48-hourly precipitation.

Temperature is an important driver of evapotranspiration that also captures seasonal features of flooding. Temperature data comes from the CPC Global Daily Temperature data from the NOAA (National Oceanic and Atmospheric Administration et al. 2021) and the dataset contains global gridded daily minimum and maximum temperatures at a resolution of $0.5° \times 0.5°$ from 1979 to the present. Because temperature resolution is lower than precipitation, we downscaled the data to $0.1° \times 0.1°$ assuming constant average daily temperature within each block of 5x5 grid cells. This is a reasonable assumption given that spatial variations of temperature are typically much smaller than precipitation. We built temperature covariates by recording the monthly average of daily minimum and maximum temperature per grid cell.

In Northern or alpine climates rapid snowmelt and rain-on-snow events caused by e.g., heavy rain (and rapid increases in temperature) are drivers of flooding. Therefore, we add snow cover data in the analysis from the Canadian Centre for Climate Services available over North America at a resolution of 24 km x 24 km (Ross and Bruce 2010). Snow cover data has been reprojected with bilinear interpolation to the $0.1° \times 0.1°$ grid that we use for the analysis. Every month, we recorded the daily maximum snow cover.

There are many common climate types in the U.S. and Canada, and we aimed to distinguish pluvial flooding dynamics based upon such climates using the Köppen-Geiger (KG) climate classification. There are 30 climates spread over 5 main climate groups (tropical, dry, temperate, continental, polar). KG climate classification is available as a static variable on a $0.1° \times 0.1°$ global grid (Peel, Finlayson, and McMahon 2007). Climate classification is not meant to be dynamic but rather to distinguish geographical areas based on weather patterns. Therefore, we assume it remains constant during the study period.

3.1.3 Socioeconomic variables

Land use is an important driver of flooding determining how rainfall runs off from the surface. Urbanization has led to an increase in flooding in the past (Feng, Zhang, and Bourke 2021) by limiting infiltration and increasing surface runoff. We utilize the land use data from the Commission for Environmental Cooperation (CEC 2015), which was derived from Landsat satellites data in 2015 at a resolution of 30m x 30m.

Land use is sorted into 19 classes. For each $0.1° \times 0.1°$ grid cell there are over 100,000 observations of land use. We have therefore computed the proportion of each land use type for each of the 19 classes assuming it did not change significantly over the 14 years of the study. For parsimony, we grouped 11 types of land use together, leaving us with 8 categories overall: forest, scrub, grassland, wetland, cropland, dry land, urban area and water.

As floods are only reported when there is population and because we lack appropriate projections of land use for the future, we have also included population data into the analysis. We used the U.S. Census Grid population data available for the years 2000 and 2010 from the Socioeconomic Data and

Applications Center (SEDAC) hosted at Columbia University (Seirup and Yetman 2006; CIESIN 2017). The 30 arc-second (about 1 km) grid of the U.S. Census was then aggregated at a $0.1° \times 0.1°$ resolution. A linear interpolation was used to deduce population for 2007 to 2009 and it was assumed fixed as of 2010 between 2011 and 2020 because 2020 population data was not available at the time of study. Note that gridded population data is approximately equivalent to population density since the grid cell size remains constant at $0.1° \times 0.1°$.

3.2 Methods

Flood occurrence is a classification problem and as such, we have used the Generalized Linear Model (GLM) (namely, the logistic regression), the Generalized Additive Model (GAM) and Random Forests (RF). We focused on the latter methods because the resulting models are flexible allowing for non-linearities (GAM, RF) and interactions (RF), while being interpretable. More details about GLM, GAM and RF methods can be found in Chapters 4, 7 and 8 of Gareth James et al. 2021.

The historical occurrence data described in Section 3.1.1 has more than 2.4M observations of which, 0.27% are ones (pluvial flood observed in a given month and grid cell) and the rest are zeroes (no pluvial flood observed in a given month and grid cell). As such, the dataset is imbalanced and we focus on avoiding problems related to the overestimation of the probability of no flood (false negatives).

There are few solutions to deal with data imbalance (Ganganwar 2012). It is possible to oversample ones or undersample zeroes. Given the size of the dataset, undersampling zeroes was a better option than oversampling ones, which reduces its size and accelerates computations. In other words, we randomly (over months and grid cells) eliminated zeroes from the dataset to match a given proportion of either 90% or 50%. We tested two proportions to determine whether the outcomes are sensitive to such choice. Whenever undersampling was used, predicted flood occurrence probabilities were adjusted following Saerens, Latinne, and Decaestecker 2002 to match observed probabilities.

3.3 Models

The response variable is flood occurrence in the United States, measured over grid cell-months. We assume that given a set of covariates, flood occurrence is independent (over grid cells of $0.1° \times 0.1°$ and months) and as such, this classification problem can be treated as a very typical one. The set of covariates are (as described in Section 3.1): 5 precipitation variables (6-hourly, 9-hourly, 12-hourly, 24-hourly, 48-hourly), temperature, snow cover, climate classification, 8 proportions of land use, and population density.

To eliminate the adverse effects of multicollinearity, we also built a smaller set of covariates. Indeed, we found high correlation in the precipitation variables (by construction, one being often included in the other) and only kept the 24-hour precipitation since higher frequency precipitation is not available in the climate model projections described in Section 4.1. Moreover, we found high correlation between monthly temperature and snow cover, and the latter has been excluded since temperature is also readily available in climate models whereas snow cover is not. We also found high correlation between the proportion of urban extent (one of the land use covariates) and population density and decided to keep the latter since it is readily available in future population projections. We also combined forest and grassland proportions into one for similar reasons. Overall, the smaller set of covariates comprises of: 24-hour precipitation, average daily temperature, climate classification, 5 proportions of land use (combining forest and grassland, dropping water and urban extent) and population density.

Given the imbalance dataset problem and correlation between many of these covariates (especially between the precipitation variables), we analyze each of the following using either the GLM, GAM and RF, resulting in 15 models overall:

- All covariates, no undersampling;

- All covariates, undersampling with 90% of zeroes;
- All covariates, undersampling with 50% of zeroes;
- Smaller set of covariates, undersampling with 90% of zeroes;
- Smaller set of covariates, undersampling with 90% of zeroes, with logged population density.

3.4 Validation

We first fit the 15 flood occurrence models (described in Section 3.3) over the United States with 70% of data and assess the predictive capability using a test set made of the remaining 30% (Section 3.4.1). The test set has been generated by randomly selecting 30% of data over grid cells and months of the original dataset. Fitting is then performed in `R` using: the `lm` function (GLM) from the `base` package; the `bam` function (GAM) from the `mgcv` package (Wood 2017) and, the `ranger` function (RF) from the `ranger` package (Wright, Wager, and Probst 2020). The GAM was fitted with cubic regression splines for non-factorial variables.

A model fitted over the United States (with Canadian KG climates available in the U.S.) is then used to predict pluvial flooding in Canada. The model quality over Canada is investigated in two different manners (Section 3.4.2). First, by using flood claims data from a major Canadian insurance company, yielding a purely out-of-sample predictive analysis. Second, we perform a qualitative assessment of the model over major flood events in Canada.

3.4.1 United States

We compute the areas under the receiver operating characteristic (ROC) and precision-recall (PR) curves with the test set in the United States. The results are shown in Table 1 noting that "u/s" stands for undersampling. For more details about the ROC, precision and recall metrics, the reader should refer to Chapter 4 of Gareth James et al. 2021.

Table 1. Area under the ROC (Panel A) and PR (Panel B) curves with the test set over the United States for all 15 models considered

	Panel A: ROC curve			**Panel B: PR curve**		
Models	GLM	GAM	RF	GLM	GAM	RF
All, no u/s	0.8890	0.9076	**0.9224**	0.0587	0.0762	**0.1091**
All, 90% u/s	0.8992	0.9084	**0.9254**	0.0587	0.0742	**0.0923**
All, 50% u/s	0.9017	0.9085	**0.9216**	0.0566	0.0701	**0.0766**
Smaller, 90% u/s	0.8894	0.8987	**0.9273**	0.0499	0.0653	**0.0957**
Smaller, 90% u/s, log pop	0.8969	0.9038	**0.9272**	0.0564	0.0676	**0.0957**

We find that models perform very well in the test set with an area under the ROC curve in the range of 0.89-0.93, with a slight advantage to random forests. As for the area under the PR curve, values range from 0.05 to 0.11, which is above the baseline for a non-informative model (0.005, computed with historical occurrences). The GAM model performs better than the GLM while RF again shows the best predictive capability in the test set. Overall across models considered, RF yields the largest area under both the ROC and PR curves.

It also appears from Table 1 there is no clear advantage from a predictive standpoint to undersample zeroes. When using all covariates, undersampling with a target 50% or 90% of zeroes provided a very similar area under the ROC curve for the GLM, GAM and RF. The latter result is different though for the PR curve, where undersampling slightly worsens predictive capability for the GAM, and more significantly for the RF. That being said, the more parsimonious models with undersampling still yielded very comparable performance to cases without undersampling. When computation times

matter, undersampling the dataset and using less covariates therefore yield very similar predictive performance (in a shorter amount of time and memory).

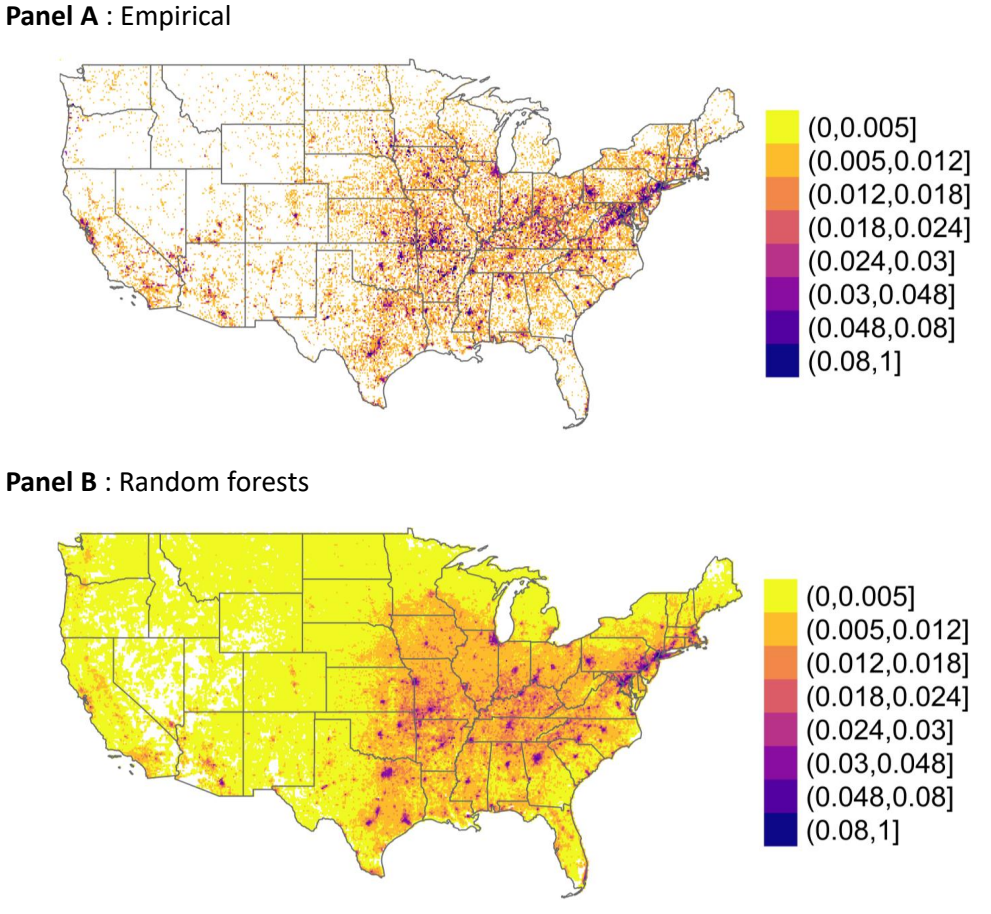

Figure 2. Flood probabilities over the United States: empirical (Panel A, top) vs predicted (Panel B, bottom) using the random forests model (undersampling with 90% of zeroes, smallest set of covariates, logged population). Similar plots for GLM and GAM available in the SM. Color scale is the same for all plots to allow comparison between models.

We compare in Figure 2 the predicted probabilities from the RF model with historical flood probabilities. That is, Panel A of Figure 2 computes the empirical flood probability per grid cell, calculated as the number of months with flood occurrence over the total number of months. A white cell means no occurrence has been observed. Panel B of Figure 2 computes the average (over months and years between 2007 and 2020) predicted flood probabilities over the United States for one random forests model (undersampling with 90% of zeroes, smallest set of covariates, logged population).

We see that pluvial flood occurrence is concentrated in urban areas and that the model does very well in characterizing the spatial characteristics of pluvial flood, which is important to distinguish where climate change might have a greater impact. In the case illustrated here, the RF appropriately

captures areas of low risk (white on top vs yellow in the bottom) and pluvial flood probabilities in urban areas are at very similar levels and locations in both panels.

The Supplementary Material (SM) includes 15 plots, one per model (GLM, GAM, RF) and one per set of covariates (5), plus the empirical probability. They show that adding the logged population density was important for GLM and GAM since it appears that predictions were too sensitive to slight changes in population otherwise.

3.4.2 Canada

We would like to perform a validation exercise of the 15 models but over Canada. There are however no formal datasets in Canada that records flood events (or other weather events) at a level of granularity that we can find in the NOAA SED (with latitude and longitude of location). The Canadian Disaster Database (Canada 2022a), maintained by Public Safety Canada, has approximately the same level of information as the EM-DAT dataset (Guha-Sapir, Below, and Hoyois 2022). The Flood List website (Davies, Behrend, and Hill 2021) also provides information about flooding globally, but in all three cases, location information is much too vague to be able to formally validate the flood models.

We thus perform a quantitative and a qualitative validation of the models over Canada. The quantitative assessment was based on a sample (non-random and non-divulged in this article) of data from Co-operators, a Canadian insurance company part of the top six P&C insurers in Canada. Data specific to clients was not used for this analysis, only aggregate information about a flood event. Such assessment is feasible since the predictors presented in Section 3.1 are available globally or over North America, with the exception of population which covers the U.S. only. In this case, we used the Gridded Population of the World (GPW) v4.11 also available from the SEDAC (CIESIN 2018).

We have also recalibrated the 15 models over the U.S. but only over regions whose Canadian KG climates are available in the U.S. (therefore excluding areas whose climate would not contribute much in predicting flood dynamics in Canada such as Southern U.S. states). As such, we show ROC and PR metrics with the claims data available from 2012 to 2020. The qualitative assessment compares time series of predicted flood probabilities between 2007 and 2020 with major historical flood events that took place over Toronto (2013, 2018) and Calgary (2013, 2019).

Table 2. Area under the ROC (Panel A) and PR (Panel B) curves with flood claims from a Canadian insurer (2012-2020) for all 15 models considered

	Panel A: ROC curve			**Panel B: PR curve**		
Models	GLM	GAM	RF	GLM	GAM	RF
All, no u/s	**0.8136**	0.7812	0.7994	0.0153	0.0258	**0.0301**
All, 90% u/s	0.8065	0.7816	**0.8158**	0.0102	0.0236	**0.0339**
All, 50% u/s	0.7867	0.7811	**0.8147**	0.0077	0.0226	**0.0267**
Smaller, 90% u/s	0.7740	0.7874	**0.8276**	0.0094	0.0243	**0.0274**
Smaller, 90% u/s, log pop	**0.9009**	0.8219	0.8281	0.0152	0.0164	**0.0269**

Table 2 shows the area under the ROC and PR curves for the 15 models applied in Canada. In bold face we highlight the method with the highest metric in each line. We now see a different picture, as is usually the case when performing out-of-sample prediction exercises. The areas under the ROC curves now range within 0.77-0.90 which is lower than what we obtained over the United States. That being said, the performance is very good especially for the models with the smallest set of covariates and logged population, with metrics in the range of 0.83-0.90. It is particularly surprising to observe a value of 0.9 with the fifth model under the GLM; it appears that simpler specifications are performing well out-of-sample in Canada and that logged population captures the

fact that urbanization beyond some level should not have the same impact on pluvial flood probability. We therefore have a solid case for the fifth set of models (smaller set of covariates, undersampling with 90% of zeroes, with logged population density) which has the highest scores while being the fastest to fit (because of fewer covariates and smaller sample size due to undersampling). As for the areas under the PR curves, it shows that the random forests models have a slight advantage over the GAM.

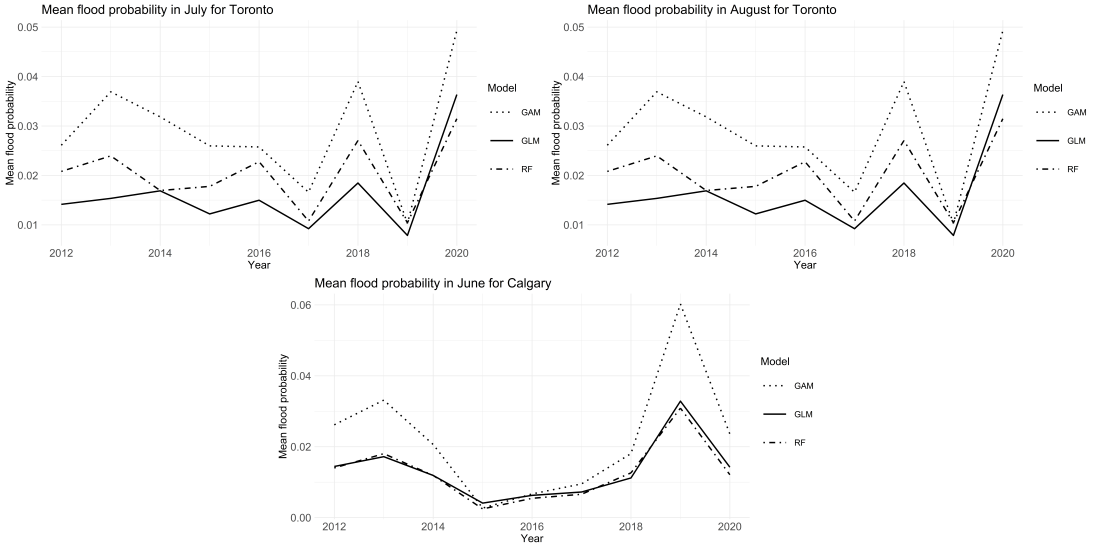

Figure 3. Validation of pluvial flood models with predicted flood probabilities in Toronto over July and August (top row), and Calgary over June (bottom row) between 2012 and 2020. Models with the smallest set of covariates, 90% of zeroes and logged population density were used.

We continue this section with a qualitative assessment of the models using selected flood events in Canada. We have plotted in Figure 3 the predicted pluvial flood probability over the months of July and August in Toronto (top row). We observe major peaks in probabilities in July and August 2013 as well as in August 2018 which coincide with major flooding events in downtown Toronto. The 2013 floods in Toronto were among the most expensive for the insurance industry in Canada.

Figure 3 also shows a similar plot for Calgary in June of very year of the sample (bottom row). We can distinguish significant peaks over June 2013 and June 2019. Although heavy rain triggered flooding in Calgary in June 2013, heavy snow accumulation upstream in the prior months magnified the intensity of the event, which might explain why the maximum observed in 2019 is higher than in 2013, because of the longer term snow melt processes. Calgary also saw floods in June 2019 due to thunderstorms pouring in largely abnormal amounts of rain.

Moreover, in the three subplots of Figure 3, we observe that the GAM typically generates the largest range of flood probabilities, indicating the model is the most responsive to changes in precipitation patterns. Finally, on the basis of the quantitative and qualitative validations, we are comfortable in saying the pluvial flood model fitted in the United States provides strong predictions in Canada.

We conclude this section by providing a map of pluvial flood probabilities over Canada. Figure 4 shows the predicted pluvial flood probabilities (averaged over years and months between 2007 and 2020) from the random forests model (Panel A, top) and the GLM (Panel B, bottom) using undersampling with 90% of zeroes, the smallest set of covariates and logged population. Pluvial flooding is therefore also concentrated in urban areas as was the case for the United States. This is

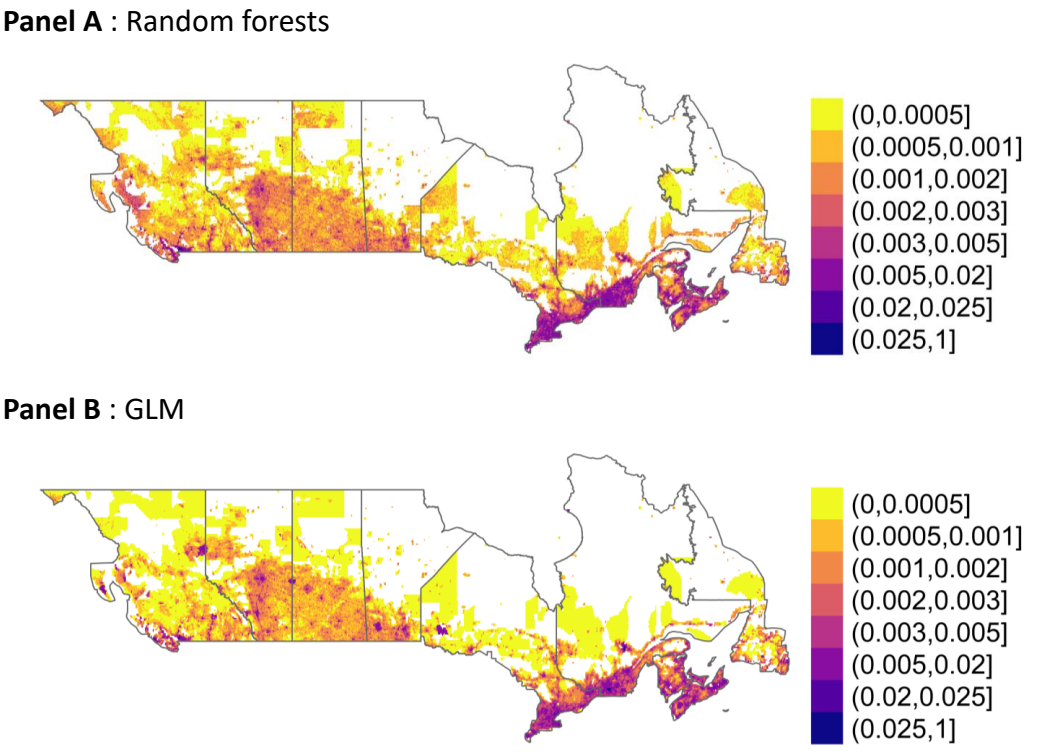

Figure 4. Predicted flood probabilities over Canada for the random forests model (Panel A, top) and GLM (Panel B, bottom) using undersampling with 90% of zeroes, the smallest set of covariates and logged population. Note that we cannot show historical flood probabilities to protect the confidentiality of the data. Similar plots for GAM are available in the SM. Color scale is the same for all plots to allow comparison between models.

especially true in the Greater Vancouver area, Southern Quebec and Ontario (including, Montreal and Toronto), as well as many urban areas of New Brunswick and Nova Scotia. Note that we cannot show historical claims patterns in Canada to protect the confidentiality of the clients. Moreover, we have more blank cells in Canada because more cells have no population (or too few) and because Northern Canadian climates could not be found in the U.S.

4. Future projections

In this section, we analyze pluvial flood probabilities predicted for the future. We first discuss the datasets used to build covariates (Section 4.1), then how the statistical and machine learning methods have been applied with such covariates (Section 4.2). We conclude this section by analyzing the impacts of climate change and urbanization on pluvial flooding over the United States, Canada and for selected cities of both countries (Sections 4.3 and 4.4).

4.1 Data

4.1.1 Climate models outputs

We used climate model simulations from the Canadian Regional Climate Model version 5 (CRCM5) (Šeparović et al. 2013; Martynov et al. 2013) available from the Coordinated Regional Climate Downscaling experiment (CORDEX) - North America (NA) ensemble (World Climate Research Programme, WCRP). The six CRCM5 runs used are: CCCma-CanESM2, MPI-ESM-LR, MPI-ESM-MR, UQAM-GEMatm-Can-ESMsea, UQAM-GEMatm-MPI-ESMsea and UQAM-GEMatm-MPILRsea. The domain covers Canada and the U.S. at a spatial resolution of 0.22° (about 25 km) from 1850 to 2100. Contrarily to GCMs, RCMs better capture local dynamics than statistical downscaling (Maraun and Widmann 2018). The CRCM5 is also well known to simulate precipitation extremes, which is an important feature to model pluvial flooding (Martynov et al. 2013; Martel, Mailhot, and Brissette 2020).

We extracted data from 2007 to 2060 to match the initial date of the NOAA SED with an approximate 40-year future time horizon. Projections beyond 2060 are highly uncertain and heavily depend on climate policies enacted today. All runs were forced with the RCP 8.5 scenario starting from 2006 (and historical emissions before 2006) which assumes that emissions continue until 2100. Our analysis is focused on short term projections (2010-2030, centered on 2020) and medium-term projections (2040-2060, centered on 2050). Until 2060 the concentration scenarios do not differ much but RCP 8.5 still represents a pessimistic scenario.

Daily precipitation in the CRCM is expressed in $kgs^{-1}m^{-2}$ and temperature in degrees Kelvin. We multiplied precipitation by 86,400 to convert precipitation into mm/24hr and subtracted 273.15 to convert temperature into degrees Celsius.

4.1.2 Socioeconomic projections

Population projections for the future are also available from the SEDAC (Jones and O'Neill 2020). These projections are typically consistent with GHG emissions scenarios used in climate models. As such, we used two population projections, that are derived from the Shared Socioeconomic Pathways (SSP) scenarios from the IPCC (IPCC 2022). We applied the SSP2 and SSP5 scenarios which are respectively labelled as "Middle of the Road" and "Fossil-fueled Development" (O'Neill et al. 2014; Fricko et al. 2017; IPCC 2022). Both of these population projections are available on a $0.125° \times 0.125°$ grid and were reprojected to match the grids of the climate models.

4.2 Methods

Because hourly precipitation is not available in the CRCM5 runs we analyzed, not all 15 models from Section 3.3 will be used for climate change risk assessment. Due to the unavailability of some

variables, the predictive capability of the models, and computation times, we used the smaller set of covariates along with a targeted 90% of zeroes for each of the GLM, GAM and RF. Covariates thus comprise: 24-hour precipitation, temperature, climate classification, 5 proportions of land use and population density.

The first step is updating our covariates using the climate model. For each of the six runs of the CRCM5 over 2006 until 2060, we extract 24-hour precipitation and compute the average daily temperature. Afterwards, we record the maximum daily precipitation over the month and compute the average monthly temperature. The static variables such as Köppen-Geiger climate classifications and proportions of land use were held fixed until 2060 because no future projections were available. As for population density, we used two different assumptions: SSP2 population projections until 2060 or fixed as of 2020 (SSP5 was also considered but results were not materially different over the time horizon considered). The latter thus fixes land use and urban extent and allows us to focus strictly on changes in future atmospheric conditions whereas the former allows for interactions between increased urbanization and possibly more heavy rain.

The second step is computing flood probabilities with the updated covariates. For each month (12), year (54) and run (6) of the CRCM5, we computed flood probabilities using outputs of the CRCM5 as simulated covariates. We call these *simulated* probabilities of flooding and they are available over the present and future climates. We interpret climate simulations over the present climate as alternate and plausible trajectories of the climate.

To mitigate the need to apply some kind of post-processing (see Section 2.2) on flood probabilities, our analyses focuses on *differences* between two time periods (rather then looking at raw probabilities), therefore assuming that any bias found in the CRCM5 over the historical period is likely to be of a similar order in future projections. Appendix 1 provides an analysis of the CRCM5 over 2007-2020 and we find that such bias is very small in most areas.

4.3 Maps

The first step of our analysis is to compare flood probabilities between two time periods: 2010-2030 (centered on 2020) and 2040-2060 (centered on 2050), which are 30 years apart. We therefore average simulated probabilities across months, years and runs of each time period. Figure 5 shows the difference in pluvial flood probability between 2040-2060 and 2010-2030 for the United States for the GLM (Panel A, top), GAM (Panel B, middle) and RF (Panel C, bottom). Figure 6 is similar to Figure 5 but for Canada. Both plots therefore highlight the combined impacts of climate change and future urbanization on the pluvial flooding hazard.

Whereas all three models agree that the West Coast of the U.S. and Canada will be the most affected by changes in flood probabilities, there are however large discrepancies between predictions of the GAM/GLM and the random forests. The GAM/GLM families of models yield increases of pluvial flooding elsewhere in the U.S. and Canada, concentrated in urban areas of Eastern U.S. and Southern Quebec and Ontario, whereas the random forests method shows close to no changes elsewhere. In fact, the random forests show the smallest increases over the West Coast.

One should be very careful with the results from the random forests because it is well known that RF and tree-based methods are unable to extrapolate beyond the range of the training set (Hengl et al. 2018). This becomes a major issue for climate change risk assessments because atmospheric variables such as precipitation and temperature patterns in the future may very well be much different from their equivalent in the past.

4.4 Select cities

The inability of the RF to extrapolate beyond the original training set becomes obvious when we look at time series of simulated probabilities of flooding from 2006 to 2060 for select cities in the United States and Canada. Figure 7 shows the average (taken over months, grid cells of the city and

Panel A : GLM

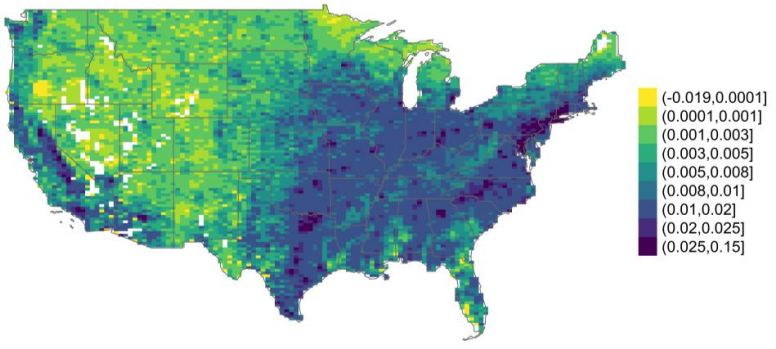

Panel B : GAM

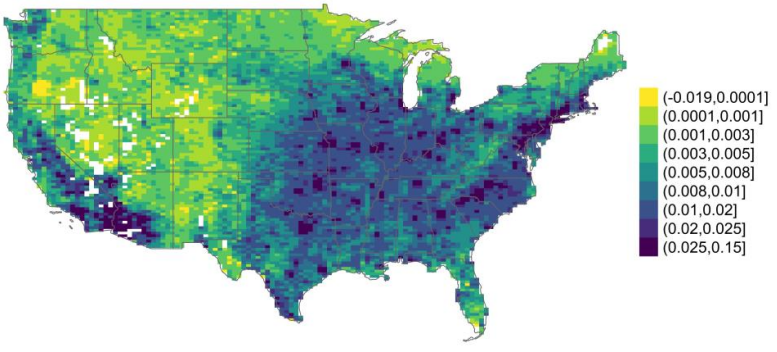

Panel C : Random forests

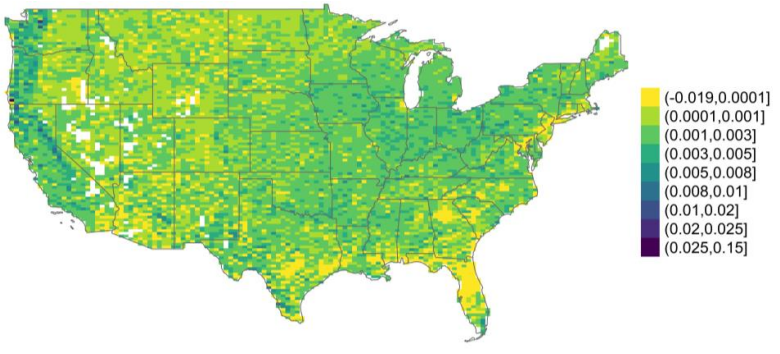

Figure 5. Difference in simulated pluvial flood probability between 2040-2060 and 2010-2030 computed with the GLM (Panel A, top), GAM (Panel B, middle) and RF (Panel C, bottom) models over the United States. Color scale is the same for all plots to allow comparison between models.

Panel A : GLM

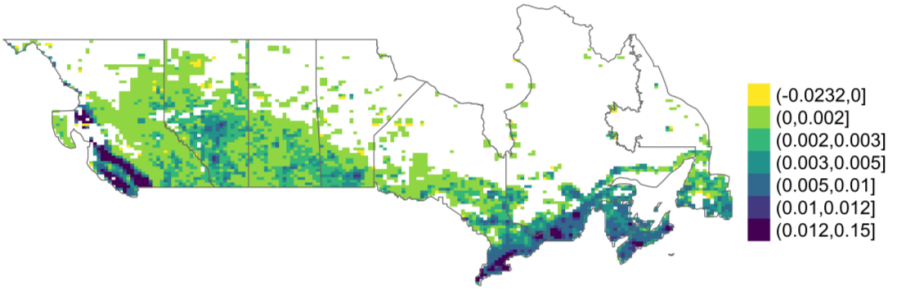

Panel B : GAM

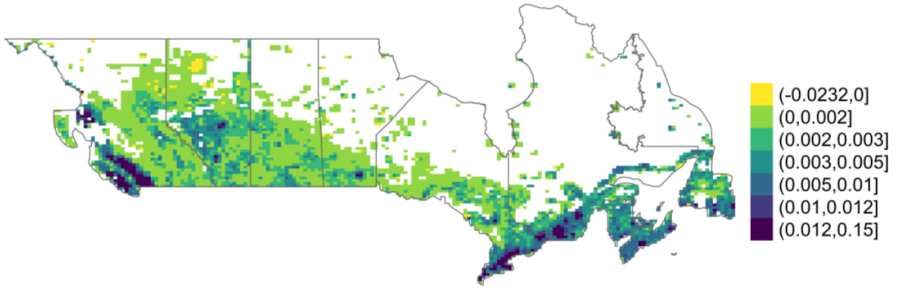

Panel C : Random forests

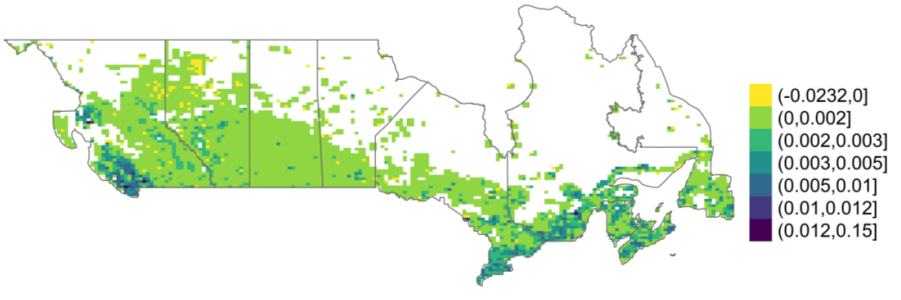

Figure 6. Difference in simulated pluvial flood probability between 2040-2060 and 2010-2030 computed with the GLM (Panel A, top), GAM (Panel B, middle) and RF (Panel C, bottom) models over Canada. Color scale is the same for all plots to allow comparison between models.

the six runs of the CRCM) annual simulated pluvial flooding probability over New York, Houston, Chicago and Denver with the GAM (Panel A, top) and RF (Panel B, bottom) respectively. First of all we observe an increasing trend of different slopes with the GAM and nearly no trend with the RF. Even though we averaged results over the six runs, there is still substantial interannual variability, well illustrated with the GAM but not much with the RF.

In Figure 7, we also isolated the effects of climate change from increased urbanization with the continuous and dotted lines. That is, the dotted line represents a scenario where population remains fixed after 2020, whereas the continuous line represents a scenario where population increases according to the SSP2 scenario. In the latter scenario, the population of New York, Chicago and Denver will continuously increase in the future, whereas Houston should see a population decrease from 2020 to 2030 and an increase thereafter. Although the increasing trend in flood probability seems primarily driven by changing patterns in temperature and precipitation, urbanization also plays an important role on flood hazard.

Finally, Figure 8 shows a similar plot for Montreal, Toronto and Vancouver with steep increases and impact of urbanization. The SM includes plots for the GLM over the same select U.S. cities, and two plots, for three Canadian cities with the GLM and RF.

5. Portfolio applications

We present in this section portfolio applications of the pluvial flood occurrence model under various hazard and exposure scenarios. This section has three objectives: (1) to demonstrate how the overall methodology could be used for PRA; (2) to differentiate the impacts of changes in hazard and exposure and their interaction on portfolio losses, and; (3) to illustrate spatial heterogeneity of future climate and population projections.

5.1 Methodology

The occurrence model applied to the CRCM5 and SSP2 population projection yields simulated flood probabilities for each grid cell, month and year between 2006 and 2060. We can therefore easily use these probabilities to simulate monthly flood occurrences over the future. But an important piece remains, linking flood occurrence to impact in terms of losses.

With hazard information available at a resolution of 10–25 km, we will not aim to analyze impacts at the street level, and as such, exact location of each building is not necessary for this exercise. For similar reasons, we will also ignore the vulnerability of each building, and rather assume that each flooded property suffers a fixed or random loss amount. Aggregating exposure value, or the number of households insured per grid cell at a resolution similar than the climate model is straightforward for an insurer. But for this paper, we will rather build generic insurance portfolios based upon the population data described in Sections 3.1 and 4.1.

It remains to determine the number of homeowners that are flooded when there is flood occurrence in a given grid cell. One can fix that number as a given percentage but we instead modelled that as a beta distributed random variable with fixed mean and a fixed upper percentile. As such this adds randomness as to how extreme precipitation may locally affect a community.

The specific methodology is as follows. We have split the time horizon until 2060 into two time periods: present climate (2010–2030), centered around 2020 and future climate, centered around 2050 (2040–2060). A 30-year time horizon is reasonable for an insurer for strategic decision-making and solvency analyses and also avoids a considerable amount of uncertainty tied to climate up to 2100 which is heavily dependent upon current climate policies. Each model run (6) and year (20) within each time period is assumed to be independent and identically distributed. This yields 120 climate simulations under the present climate, and also an extra 120 climate simulations under the future climate.

Panel A : GAM

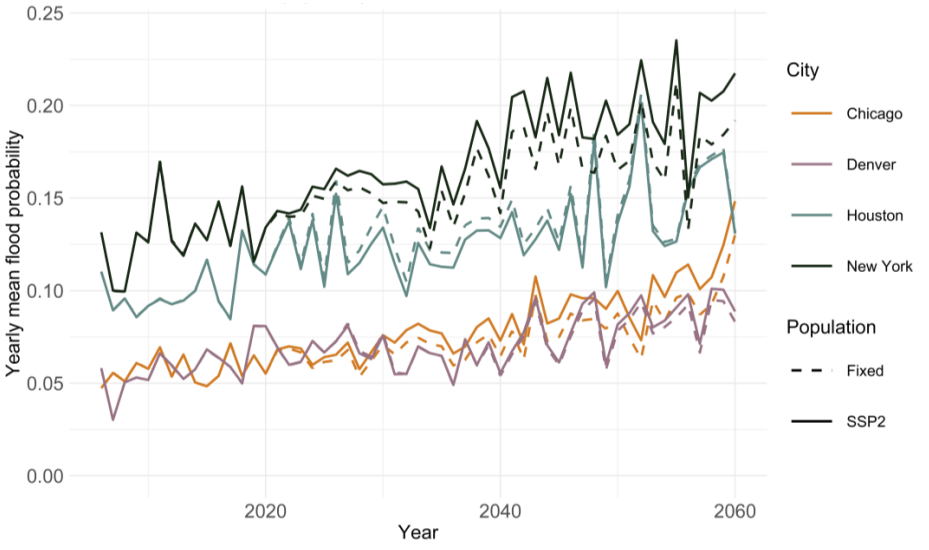

Panel B : Random forests

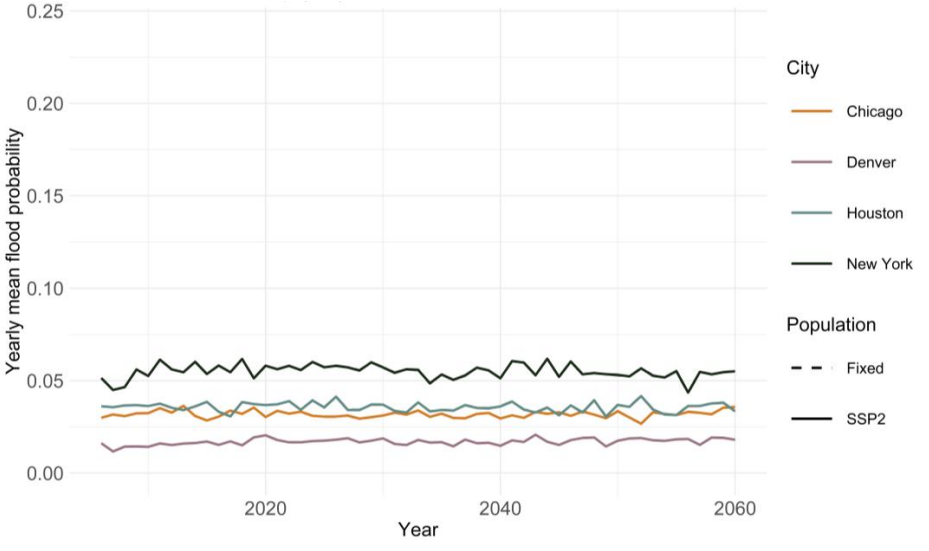

Figure 7. Annual simulated pluvial flood probability from 2006 to 2060 over New York, Houston, Chicago and Denver with the GAM (Panel A, top) and RF (Panel B, bottom). GLM available in the SM.

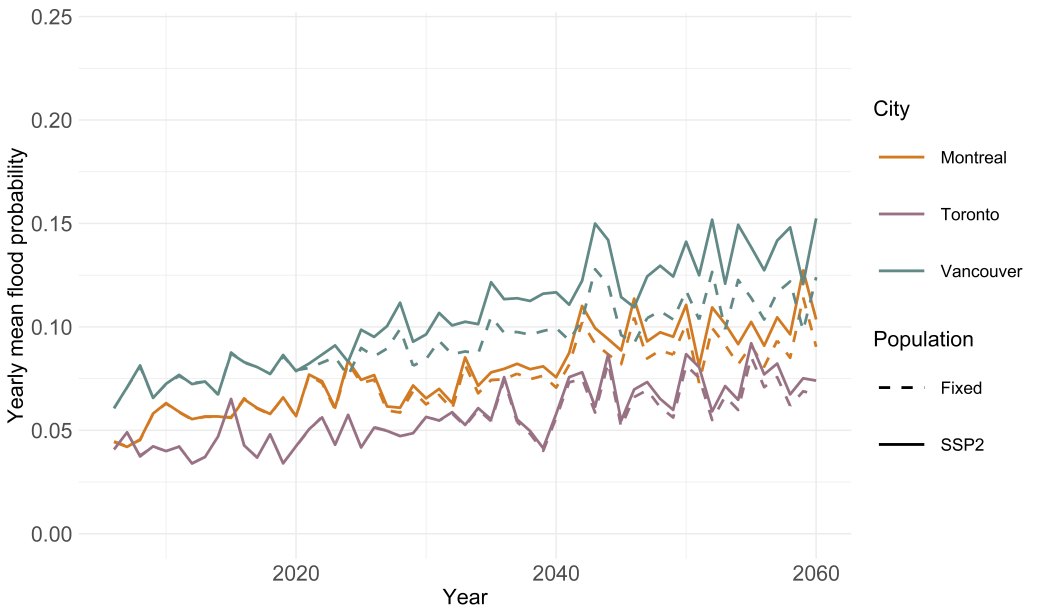

Figure 8. Annual simulated pluvial flooding probability from 2006 to 2060 over Montreal, Toronto and Vancouver with the GAM model. Similar plots for GLM and RF are available in the SM.

For the present climate, we draw 10,000 random numbers, effectively randomly selecting a climate from the 120 available. For the selected climate, we compute simulated flood probabilities for each grid cell and month over Canada and the United States. We then draw Bernoulli random variates according to these probabilities over each grid cell assuming that flood occurrences conditional upon the climate is spatially independent. If there is a flood in a given grid cell, we then randomly draw from a beta distribution with mean 2% and 99-th percentile equal to 20%. And for each household affected by a flood, we assume losses of $25,000. The value of $25,000 is somewhat the average damage given a pluvial flood per property whereas 2% aims to replicate industry losses. If one is interested in understanding the *relative* impacts of climate change, these values do not make a material difference.

The previous steps have then been repeated over the future climate as well. In both cases, we worked with the GAM and the smaller set of covariates fitted with a targeted 90% of zeroes. GLM yields similar results whereas the RF has been excluded for reasons explained in Section 4.

5.2 Results

To meet the objectives above, we build three different scenarios for changes in the hazard and exposure. The baseline scenario represents our best estimate of the current loss distribution. It is based upon present-day hazard (2020) and exposure (2020). The second scenario assesses the sensitivity of the insurer's current exposure (2020) to changes in hazard (2050), including future projections for temperature, precipitation and urbanization. It represents what would be typically asked for reporting and regulating purposes to assess the impacts of future pluvial flood hazard. In this case, the insurer's portfolio is held fixed in the future, as if the insurer would not underwrite additional risks. Finally, the third scenario includes changes in both the hazard (2050) and exposure (2050) and depicts a situation where a company underwrites in a similar manner and fixes its future market share instead. Such a scenario also highlights possible interactions between hazard and exposure

where population could increase or decrease in riskier or safer areas. In all cases, we fixed the market share to 100% of the corresponding geographic region, which therefore proxies industry losses.

Table 3 shows the results of the latter three scenarios for four portfolios, fully underwritten in Quebec, Ontario, Canada or over the U.S. Note that $ amounts have not been adjusted for inflation and reflect losses as of 2020. All risk measures were computed with 10,000 simulations whereas the mean and standard deviations were validated with closed-form expressions that are straightforward to derive. We show in Appendix 2 the equivalent of Table 3 but for each of the 10 Canadian provinces, and the 10 most populous U.S. states.

Table 3. Portfolio loss statistics for four portfolios and three scenarios for changes in hazard and exposure (in millions of 2020 dollars). Relative difference in % shown between parentheses (compared to the baseline scenario).

	Hazard	Exposure	Average	Std. dev.	90th perc.	95th perc.	99th perc.
Quebec	2020	2020	471	653	1154	1707	3291
	2050	2020	692 (47%)	767 (18%)	1601 (39%)	2234 (31%)	3872 (18%)
	2050	2050	913 (94%)	995 (53%)	2067 (79%)	2947 (73%)	5070 (54%)
Ontario	2020	2020	693	827	1613	2291	4281
	2050	2020	1029 (49%)	987 (19%)	2243 (39%)	3059 (34%)	4827 (13%)
	2050	2050	1285 (85%)	1175 (42%)	2713 (68%)	3701 (62%)	5842 (36%)
Canada	2020	2020	1834	1260	3518	4327	6230
	2050	2020	2605 (42%)	1462 (16%)	4562 (30%)	5467 (26%)	7583 (22%)
	2050	2050	3240 (77%)	1717 (36%)	5469 (55%)	6600 (53%)	9219 (48%)
USA	2020	2020	18840	5666	26660	28948	33057
	2050	2020	24499 (30%)	6625 (17%)	32551 (22%)	35165 (21%)	42551 (29%)
	2050	2050	29775 (58%)	8261 (46%)	40112 (50%)	43508 (50%)	52036 (57%)

With the four portfolios illustrated in Table 3, we see that even in the aggregate, changes in hazard can be very different across regions. Under the second scenario (hazard of 2050 but exposure of 2020), losses are expected to increase by nearly 50% in both Quebec and Ontario, whereas the increase is lower Canada-wide (about +40%) or in the United States (+30%). Expressed differently, such increases represent 0.88% to 1.36% per year on an annual basis (annually compounded). Across states and provinces, Appendix 2 shows more homogeneity across Canadian provinces (increases of about 40-50% with the exception of BC and PEI) than in the U.S., where increases range from 15-50%.

We find benefits to diversification but still, country-wide effects of climate change on pluvial flood are expected to be more significant in Canada (relatively speaking) than in the U.S. According to ECCC (Bush and Lemmen 2019), the average temperature increase in Canada is expected to be greater than in the U.S., which in theory would mean that the air over Canada could hold more humidity that would in turn result in more intense rainfall, all other things being equal.

In the third scenario, both the hazard and exposure change in the future. There are however non-trivial interactions between changes in hazard and exposure depending on where population will live. Indeed, if for example current and future population move to areas with increasing hazard, then portfolio losses will increase at a faster pace than population growth. Table 3 shows that the third scenario yields losses much greater than the second scenario with significant heterogeneity. For example the Quebec portfolio losses nearly double while the U.S.-wide portfolio losses increase by about 60%. Expressed on an annual basis, the compounding effects of increasing hazard and exposure mean that losses should increase by a rate of 1.6% to 2.2% annually. Across states and provinces, Appendix 2 shows variations between 40-95% over Canadian provinces and the top 10 U.S. states, which is very significant.

It should therefore not be a surprise to observe a significant trend in future losses, where adding inflation of about 3% (which is slightly above the historical inflation over the last 40 years, but still below the inflation observed in 2022–2023), could yield a compound annual rate of increase in losses of over 5% (all else being equal, namely adaptation). Note that according to the Parliamentary Budget Officer in Canada, claims to the Disaster Financial Assistance Arrangements due to flooding have quadrupled over the last 40 years (Office of the Parliamentary Budget Officer 2016), and therefore, such figures are clearly not unrealistic.

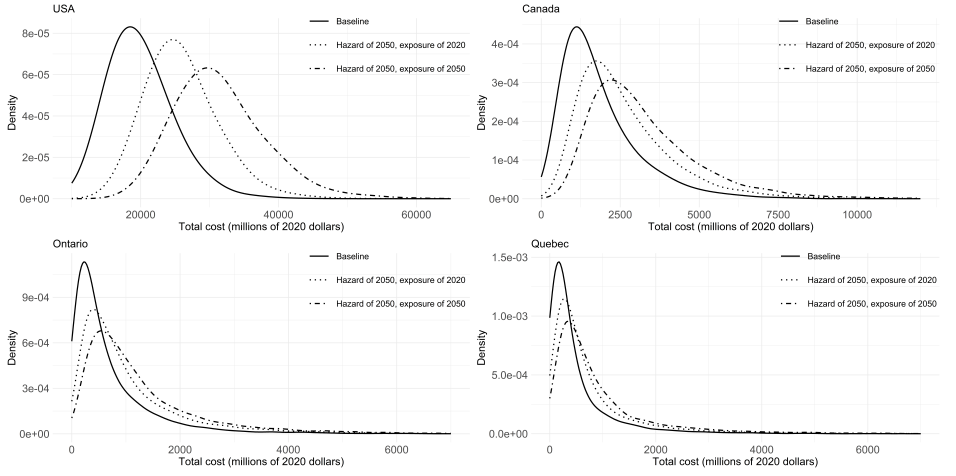

Figure 9. Probability density functions of portfolio losses for each portfolio and scenario

We conclude this section by analyzing the (kernel-smoothed) loss distributions in each of the three scenarios for the four portfolios. We clearly see in Figure 9 rightward shifts as we move from the baseline scenario (hazard of 2020, exposure of 2020) to the third scenario (hazard of 2050, exposure of 2050). The Quebec and Ontario portfolios are right-skewed and heavy-tailed, even more so than the Canadian and U.S. portfolios. Judging by the upper percentiles, there does not appear to be a thickening of the right-tail under the third scenario, but this is based upon 10,000 simulations founded on 120 different climates, which could limit the potential to capture extreme losses.

This portfolio application shows the value for (re)insurance companies to invest in better underwriting practices and/or work with communities to attenuate the financial impacts of climate change on flooding. It also highlights the importance of quantitative PRA to support such strategic decision-making at the organization level.

6. Discussion and conclusion

As reporting and regulatory requirements evolve, actuaries will increasingly need to factor in climate change into various business functions such as underwriting, reserving and strategic decision-making. Climate risks are not new to actuaries, but climate change might force the actuarial profession to not only look for answers in past data, but also look forward in the future using climate models. Integrating climate models into actuarial assessments is certainly new to the profession and this paper has showed that PRA can certainly be viewed as a data science problem. This is an important outcome given the talent pool that insurers typically recruit from.

One objective of the paper was to assess how pluvial flood risk may affect an insurance portfolio in the future. Using historical data on pluvial flood occurrences, we applied statistical and machine learning methods to better understand the relationship between these flood occurrences and atmospheric and socioeconomic variables (fitting and validation step). Using climate model outputs as

simulations of atmospheric variables over the present and future, we then computed pluvial flood probabilities over Canada and the United States until 2060 (projection and simulation step). Finally, with a simple portfolio model founded on one flood occurrence model, we evaluated how changes in hazard and exposure may impact different insurance portfolios. The overall approach depicted in the paper is meant for large-scale applications that do not necessarily require street-level information, as is often the case for scenario and trend analyses. There is obviously a trade-off between speed, cost and precision for all applications, and the methodology described here is no exception.

We found that standard statistical and machine learning methods such as GLM, GAM and RF are very good at predicting pluvial flood occurrence over the United States and that such fit also yields solid predictive skill out-of-sample over Canada. We used six runs of the CRCM5 regional climate model available in the CORDEX-NA ensemble to compute flood probabilities over the United States and Canada. We found strongly heterogeneous impacts of climate change over urban areas in Canada and the United States. Results are consistent whether we use GLM or GAM to explain the link between atmospheric variables and flood occurrences, but random forests are clearly not recommended for climate change risk assessments due to their inability to make reliable predictions outside of their training domain. Predicted flood probabilities from the RF for future climates go against the mounting evidence that climate change will increase heavy rain episodes and pluvial flooding (IPCC 2022; Bush and Lemmen 2019).

Long-term PRA yields many uncertainties that stem from the natural variability of climate, the complexity of natural hazards and also the unpredictable future climate policies and resulting GHG emissions. To assess the size and impact of such uncertainties, one approach is to evaluate the sensitivity of the results to different emissions scenarios (RCPs and SSPs) and different classes of models (higher resolution GCMs from the CMIP6 ensemble used in the AR6 of the IPCC). This is left for future research. And given a sample made of 168 grids of 143,922 cells or 2.4M observations, it would be interesting to evaluate deep learning methods and their ability to extrapolate out-of-sample over Canada and over future climates. This is also left for future research.

Acknowledgement

The authors would like to thank Philippe Lucas-Picher for reviewing the manuscript, and Jean-Philippe Boucher and Mathieu Pigeon for their comments on earlier versions of this work. We would like to highlight the support from Jacob Chenette for finetuning the figures.

Funding Statement This research was supported by a Mitacs Accelerate Grant (IT14293) partly funded by Co-operators General Insurance Company. This research was also supported by the Natural Sciences and Engineering Research Council of Canada (NSERC) through a Discovery Grant (Mathieu Boudreault, RGPIN-2021-03362).

Competing Interests None.

Appendix 1. Bias analysis

To determine if the CRCM5 generates important biases in flood probabilities, one can compare *simulated* flood probabilities (with predictors computed from the CRCM5) with *predicted* flood probabilities (with predictors computed from observations). We have done such an exercise with the GLM, GAM and RF models over the common time period of 2007-2020.

Table 4 provides the distribution (over grid cells) of that difference in probabilities across the United States and Canada, and over the three models. We observe that about 1% of grid cells yield negative differences, meaning about 99% of grid cells are overestimated with the CRCM5. However, the size of the overestimation remains manageable, since for the random forests, 99% of the area

Table 4. Quantiles of the difference between simulated (from the CRCM) and historical flood probabilities using the GLM, GAM and RF models over the United States and Canada

	GLM		GAM		RF	
Quantiles	USA	CAN	USA	CAN	USA	CAN
0.1%	-0.4132%	-1.2933%	-0.2331%	-0.2821%	-1.7778%	-0.0838%
1%	-0.0114%	-0.1713%	-0.0186%	-0.1026%	-0.2936%	-0.0055%
10%	0.0638%	0.0085%	0.0476%	0.0024%	0.0710%	0.0515%
25%	0.1557%	0.0224%	0.1244%	0.0210%	0.1673%	0.0769%
50%	0.4723%	0.0835%	0.3460%	0.0805%	0.3426%	0.1450%
75%	1.1368%	0.2168%	0.7756%	0.2277%	0.7077%	0.2973%
90%	1.9030%	0.4640%	1.5379%	0.4448%	1.1056%	0.5470%
99%	3.8756%	1.6976%	5.0825%	2.0039%	2.0511%	1.3404%
99.9%	6.1483%	6.1560%	11.8372%	6.0690%	3.0322%	2.4598%

in the U.S. yields errors smaller than 2% (1.3% in Canada). The random forest method appears to yield smaller errors, which is consistent with its predictive capability in the test and validation sets (Sections 3.4.1 and 3.4.2). Note that there are few NAs (white cells, close to no population) in the U.S. and significantly more in Canada, which could explain why errors appear smaller in Canada.

We would like to determine where errors are the smallest or the largest over Canada and the U.S. As such, Figure 10 shows the difference between the simulated flood occurrence probability (from the CRCM5) and predicted flood occurrence probability (from observations), for each grid cell, averaged over months, for the United States (Panel A, top) and Canada (Panel B, bottom) for the random forests. Similar plots for the GLM and GAM are provided in the Supplementary Material. We see that errors are in general small almost everywhere, being the largest in the greater New York and Vancouver areas. In the U.S. for example, errors are still within 1% in most key areas, that is the entire West Coast, Southern and North Eastern U.S., and within 0.3% elsewhere, namely Central U.S. In Canada, errors are the largest in South Western BC, and Southern Ontario and Quebec, in addition to New Brunswick and Nova Scotia. Overall in both countries, errors are larger in urbanized areas because their flood probabilities are larger as well.

Appendix 2. Portfolio applications

This section presents the equivalent of Table 3 for the 10 Canadian provinces (Table 5) and the 10 most populous U.S. states (Table 6).

References

Bank of England. 2019. *The 2021 biennial exploratory scenario on the financial risks from climate change.*

Beck, Hylke E., Eric F. Wood, Ming Pan, Colby K. Fisher, Diego G. Miralles, Albert I. J. M. van Dijk, Tim R. McVicar, and Robert F. Adler. 2019. MSWEP V2 Global 3-Hourly 0.1° Precipitation: Methodology and Quantitative Assessment. *Bulletin of the American Meteorological Society* 100, no. 3 (March): 473–500. ISSN: 0003-0007, 1520-0477, accessed July 29, 2021. https://doi.org/10.1175/BAMS-D-17-0138.1. https://journals.ametsoc.org/view/journals/bams/100/3/bams-d-17-0138.1.xml.

Boudreault, Mathieu, Patrick Grenier, Mathieu Pigeon, Jean-Mathieu Potvin, and Richard Turcotte. 2020. Pricing flood insurance with a hierarchical physics-based model. *North American Actuarial Journal* 24 (2): 251–274.

Bush, E., and D.S. Lemmen. 2019. *Canada's Changing Climate Report.* Technical report. Government of Canada.

Canada, Public Safety. 2022a. *Canadian disaster database.* https://www.publicsafety.gc.ca/cnt/rsrcs/cndn-dsstr-dtbs/index-en.aspx.

———. 2022b. *Floods,* August. https://www.publicsafety.gc.ca/cnt/mrgnc-mngmnt/ntrl-hzrds/fld-en.aspx.

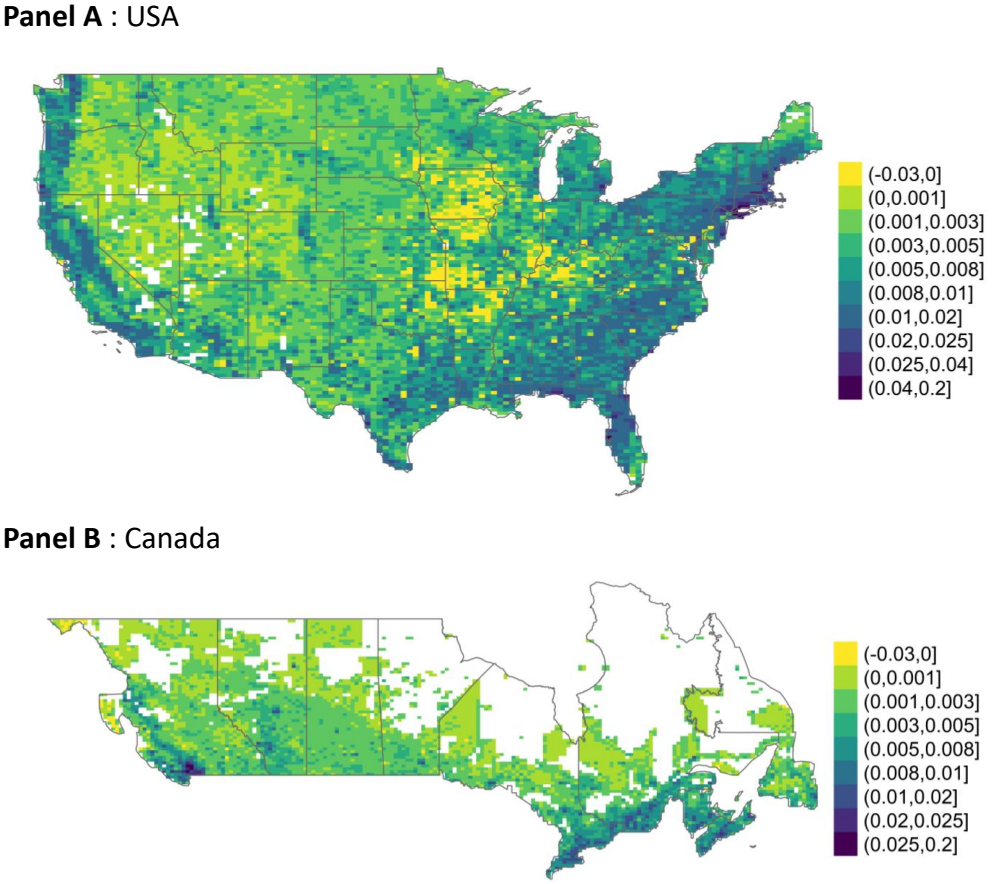

Figure 10. Difference between simulated (from the CRCM) and predicted (from observations) flood probabilities using the RF model over the United States (Panel A, top) and Canada (Panel B, bottom) and over 2007-2020. Similar plots for GLM and GAM available in the SM.

Table 5. Portfolio loss statistics for Canadian provinces and three scenarios for changes in hazard and exposure (in millions of 2020 dollars). Relative difference in % shown between parentheses (compared to the baseline scenario).

	Hazard	Exposure	Average	Std. dev.	90th perc.	95th perc.	99th perc.
	2020	2020	26	41	64	96	199
NB	2050	2020	38 (46%)	48 (18%)	89 (39%)	127 (33%)	237 (19%)
	2050	2050	43 (68%)	47 (14%)	97 (53%)	134 (40%)	223 (12%)
	2020	2020	3	12	7	17	60
PEI	2050	2020	5 (59%)	16 (24%)	13 (78%)	26 (54%)	73 (23%)
	2050	2050	6 (88%)	17 (33%)	17 (125%)	31 (83%)	79 (33%)
	2020	2020	43	84	94	163	456
NS	2050	2020	61 (42%)	97 (15%)	135 (43%)	216 (32%)	525 (15%)
	2050	2050	68 (59%)	93 (11%)	144 (52%)	218 (33%)	507 (11%)
	2020	2020	11	26	24	46	136
NL	2050	2020	16 (47%)	30 (17%)	35 (49%)	61 (32%)	156 (15%)
	2050	2050	19 (74%)	33 (27%)	42 (79%)	72 (57%)	170 (26%)
	2020	2020	26	41	64	96	199
MB	2050	2020	38 (46%)	48 (18%)	89 (39%)	127 (33%)	237 (19%)
	2050	2050	46 (78%)	49 (21%)	103 (61%)	142 (48%)	236 (18%)
	2020	2020	21	52	48	92	289
SK	2050	2020	31 (48%)	62 (18%)	75 (54%)	127 (38%)	316 (9%)
	2050	2050	38 (80%)	67 (28%)	94 (95%)	162 (75%)	341 (18%)
	2020	2020	141	273	354	581	1340
AB	2050	2020	199 (41%)	316 (16%)	493 (39%)	768 (32%)	1576 (18%)
	2050	2050	246 (75%)	352 (29%)	617 (75%)	905 (56%)	1734 (29%)
	2020	2020	389	610	998	1498	2979
BC	2050	2020	477 (23%)	648 (6%)	1143 (15%)	1737 (16%)	3376 (13%)
	2050	2050	573 (47%)	656 (8%)	1292 (30%)	1853 (24%)	3431 (15%)
	2020	2020	471	653	1154	1707	3291
QC	2050	2020	692 (47%)	767 (18%)	1601 (39%)	2234 (31%)	3872 (18%)
	2050	2050	913 (94%)	995 (53%)	2067 (79%)	2947 (73%)	5070 (54%)
	2020	2020	693	827	1613	2291	4281
ON	2050	2020	1029 (49%)	987 (19%)	2243 (39%)	3059 (34%)	4827 (13%)
	2050	2050	1285 (85%)	1175 (42%)	2713 (68%)	3701 (62%)	5842 (36%)

Table 6. Portfolio loss statistics for the 10 most populous U.S. states and three scenarios for changes in hazard and exposure (in millions of 2020 dollars). Relative difference in % shown between parentheses (compared to the baseline scenario).

	Hazard	Exposure	Average	Std. dev.	90th perc.	95th perc.	99th perc.
	2020	2020	2530	1968	5175	6469	9577
CA	2050	2020	3329 (32%)	2162 (10%)	6200 (20%)	7541 (17%)	10491 (10%)
	2050	2050	4116 (63%)	2858 (45%)	7873 (52%)	9709 (50%)	13664 (43%)
	2020	2020	3208	1556	5261	6130	7825
TX	2050	2020	3886 (21%)	1703 (9%)	6140 (17%)	7004 (14%)	8870 (13%)
	2050	2050	4639 (45%)	2035 (31%)	7271 (38%)	8359 (36%)	10502 (34%)
	2020	2020	2003	1185	3581	4263	5717
FL	2050	2020	2297 (15%)	1232 (4%)	3920 (9%)	4567 (7%)	6069 (6%)
	2050	2050	2845 (42%)	1614 (36%)	4927 (38%)	5868 (38%)	8122 (42%)
	2020	2020	1815	2155	4178	5992	10896
NY	2050	2020	2142 (18%)	2240 (4%)	4616 (10%)	6514 (9%)	11306 (4%)
	2050	2050	2619 (44%)	2682 (24%)	5719 (37%)	7852 (31%)	13367 (23%)
	2020	2020	1110	677	1998	2428	3362
PA	2050	2020	1435 (29%)	740 (9%)	2422 (21%)	2894 (19%)	3877 (15%)
	2050	2050	1718 (55%)	930 (37%)	2952 (48%)	3545 (46%)	4911 (46%)
	2020	2020	1017	943	2138	2873	4615
IL	2050	2020	1341 (32%)	1064 (13%)	2673 (25%)	3404 (19%)	5119 (11%)
	2050	2050	1637 (61%)	1427 (51%)	3356 (57%)	4369 (52%)	6833 (48%)
	2020	2020	801	519	1470	1816	2555
OH	2050	2020	1098 (37%)	592 (14%)	1879 (28%)	2242 (23%)	2997 (17%)
	2050	2050	1319 (65%)	726 (40%)	2287 (56%)	2724 (50%)	3680 (44%)
	2020	2020	1066	728	1994	2454	3609
GA	2050	2020	1314 (23%)	792 (9%)	2396 (20%)	2904 (18%)	4254 (18%)
	2050	2050	1557 (46%)	971 (33%)	2881 (45%)	3521 (43%)	5281 (46%)
	2020	2020	915	534	1657	1954	2569
NC	2050	2020	1236 (35%)	616 (15%)	2062 (24%)	2402 (23%)	3112 (21%)
	2050	2050	1417 (55%)	672 (26%)	2312 (40%)	2689 (38%)	3392 (32%)
	2020	2020	405	439	917	1251	2015
MI	2050	2020	596 (47%)	523 (19%)	1240 (35%)	1624 (30%)	2487 (23%)
	2050	2050	753 (86%)	714 (63%)	1618 (76%)	2145 (71%)	3371 (67%)

Carozza, David A, and Mathieu Boudreault. 2021. A global flood risk modeling framework built with climate models and machine learning. *Journal of Advances in Modeling Earth Systems* 13 (4): e2020MS002221.

CEC, Commission for Environmental Cooperation. 2015. *Land Cover 30m, 2015 (Landsat and RapidEye)* [in en-US]. Publication Title: Commission for Environmental Cooperation. Accessed August 3, 2021. http://www.cec.org/north-american-environmental-atlas/land-cover-30m-2015-landsat-and-rapideye/.

Chen, D., M. Rojas, B.H. Samset, K. Cobb, A. Diongue Niang, P. Edwards, S. Emori, et al. 2021. Framing, context, and methods. In *Climate change 2021: the physical science basis. contribution of working group i to the sixth assessment report of the intergovernmental panel on climate change,* edited by V. Masson-Delmotte, P. Zhai, A. Pirani, S.L. Connors, C. Péan, S. Berger, N. Caud, et al., 147–286. Cambridge, United Kingdom and New York, NY, USA: Cambridge University Press. https://doi.org/10.1017/9781009157896.003.

CIESIN. 2017. U.s. census grids (summary file 1), 2010. *Center for International Earth Science Information Network, Palisades, NY: NASA Socioeconomic Data and Applications Center (SEDAC).*

———. 2018. Gridded population of the world, version 4.11 (gpw v4.11): population count, revision 11. *Center for International Earth Science Information Network, Palisades, NY: NASA Socioeconomic Data and Applications Center (SEDAC).*

Corringham, Thomas W, F Martin Ralph, Alexander Gershunov, Daniel R Cayan, and Cary A Talbot. 2019. Atmospheric rivers drive flood damages in the western united states. *Science advances* 5 (12): eaax4631.

Davies, R., J. Behrend, and E. Hill. 2021. *Floodlist.* https://floodlist.com/data-api.

FEMA. 2005. *Reducing Damage from Localized Flooding.* Technical report. Federal Emergency Management Agency, June.

———. 2017. *Flood Insurance Reform: FEMA's Perspective.* Technical report. Federal Emergency Management Agency, March.

———. 2023. *National Risk Index: Technical Documentation.* Technical report. Federal Emergency Management Agency, March.

Feng, Boyu, Ying Zhang, and Robin Bourke. 2021. Urbanization impacts on flood risks based on urban growth data and coupled flood models [in en]. *Natural Hazards* 106, no. 1 (March): 613–627. ISSN: 1573-0840, accessed August 4, 2021. https://doi.org/10.1007/s11069-020-04480-0. https://doi.org/10.1007/s11069-020-04480-0.

Financial Stability Board. 2017. *Final report: recommendations of the task force on climate-related financial disclosures.*

Fricko, Oliver, Petr Havlik, Joeri Rogelj, Zbigniew Klimont, Mykola Gusti, Nils Johnson, Peter Kolp, Manfred Strubegger, Hugo Valin, Markus Amann, et al. 2017. The marker quantification of the shared socioeconomic pathway 2: a middle-of-the-road scenario for the 21st century. *Global Environmental Change* 42:251–267.

FSF. 2021. *The Cost of Climate: America's Growing Flood Risk.* Technical report. First Street Foundation, February.

Ganganwar, Vaishali. 2012. An overview of classification algorithms for imbalanced datasets. *International Journal of Emerging Technology and Advanced Engineering* 2 (January): 42–47.

Gareth James, Daniela Witten, Trevor Hastie, and Robert Tibshirani. 2021. *An Introduction to Statistical Learning with Applications in R, 2nd edition.* Springer.

Gershunov, Alexander, Tamara Shulgina, Rachel ES Clemesha, Kristen Guirguis, David W Pierce, Michael D Dettinger, David A Lavers, Daniel R Cayan, Suraj D Polade, Julie Kalansky, et al. 2019. Precipitation regime change in western north america: the role of atmospheric rivers. *Scientific reports* 9 (1): 9944.

Guha-Sapir, D., R. Below, and P. Hoyois. 2022. *Em-dat: the cred/ofda international disaster database.* www.emdat.be.

Hengl, Tomislav, Madlene Nussbaum, Marvin N Wright, Gerard BM Heuvelink, and Benedikt Gräler. 2018. Random forest as a generic framework for predictive modeling of spatial and spatio-temporal variables. *PeerJ* 6:e5518.

IBC. 2015. *The Financial Management of Flood Risk.* Technical report. Insurance Bureau of Canada.

ICLR. 2021. *Focus on Types of Flooding.* Technical report. Institute for Catastrophic Loss Reduction, April.

IPCC. 2021a. Annex vii: glossary [matthews, j.b.r., v. möller, r. van diemen, j.s. fuglestvedt, v. masson-delmotte, c. méndez, s. semenov, a. reisinger (eds.)] In *Climate change 2021: the physical science basis. contribution of working group i to the sixth assessment report of the intergovernmental panel on climate change,* edited by V. Masson-Delmotte, P. Zhai, A. Pirani, S.L. Connors, C. Péan, S. Berger, N. Caud, et al., 2215–2256. Cambridge, United Kingdom and New York, NY, USA: Cambridge University Press. https://doi.org/10.1017/9781009157896.022.

———. 2021b. *Hazard, vulnerability, exposure and risk.* https://www.ipcc.ch/srocc/chapter/technical-summary/ts-0-introduction/ipcc-srocc-ts_4/.

———. 2022. Summary for policymakers. In *Climate change 2022: impacts, adaptation, and vulnerability. contribution of working group ii to the sixth assessment report of the intergovernmental panel on climate change,* edited by H. O. Pörtner, D. C. Roberts, M. Tignor, E. S. Poloczanska, K. Mintenbeck, A. Alegría, M. Craig, et al., In Press. In Press. Cambridge, UK: Cambridge University Press.

Jin, Zhuoli, and Robert J Erhardt. 2020. Incorporating climate change projections into risk measures of index-based insurance. *North American Actuarial Journal* 24 (4): 611–625.

Jones, B., and B. C. O'Neill. 2020. Global one-eighth degree population base year and projection grids based on the shared socioeconomic pathways, revision 01. *Palisades, NY: NASA Socioeconomic Data and Applications Center (SEDAC).*

Kousky, Carolyn. 2022. *Understanding disaster insurance: new tools for a more resilient future.* Island Press.

Maraun, Douglas, and Martin Widmann. 2018. *Statistical downscaling and bias correction for climate research.* Cambridge University Press.

Martel, Jean-Luc, Alain Mailhot, and François Brissette. 2020. Global and regional projected changes in 100-yr subdaily, daily, and multiday precipitation extremes estimated from three large ensembles of climate simulations. *Journal of Climate* 33 (3): 1089–1103.

Martynov, Andrey, René Laprise, Laxmi Sushama, Katja Winger, L Šeparović, and B Dugas. 2013. Reanalysis-driven climate simulation over cordex north america domain using the canadian regional climate model, version 5: model performance evaluation. *Climate Dynamics* 41:2973–3005.

Mitchell-Wallace, Kirsten, Matthew Jones, John Hillier, and Matthew Foote. 2017. *Natural catastrophe risk management and modelling: a practitioner's guide.* John Wiley & Sons.

National Oceanic and Atmospheric Administration, Office of Oceanic and Atmospheric Research, Physical Sciences Laboratory, and Earth System Research Laboratories. 2021. *CPC Global Temperature data.* Accessed August 3, 2021. https://psl.noaa.gov/data/gridded/data.cpc.globaltemp.html.

NOAA, National Oceanic and Atmospheric Administration. 2021. *Storm Events Database \|National Centers for Environmental Information.* Accessed July 29, 2021. https://www.ncdc.noaa.gov/stormevents/.

O'Neill, Brian C, Elmar Kriegler, Keywan Riahi, Kristie L Ebi, Stephane Hallegatte, Timothy R Carter, Ritu Mathur, and Detlef P Van Vuuren. 2014. A new scenario framework for climate change research: the concept of shared socioeconomic pathways. *Climatic change* 122:387–400.

Office of the Parliamentary Budget Officer. 2016. *Estimate of the average annual cost for disaster financial assistance arrangements due to weather events.* https://www.pbo-dpb.gc.ca/web/default/files/Documents/Reports/2016/DFAA/DFAA_EN.pdf.

OSFI. 2023. *Guideline b-15.* Technical report. Office of the Superintendent of Financial Institutions, March.

Peel, M. C., B. L. Finlayson, and T. A. McMahon. 2007. Updated world map of the Köppen-Geiger climate classification [in English]. *Hydrology and Earth System Sciences* 11, no. 5 (October): 1633–1644. ISSN: 1027-5606, accessed August 3, 2021. https://doi.org/10.5194/hess-11-1633-2007. https://hess.copernicus.org/articles/11/1633/2007/hess-11-1633-2007.html.

PSC. 2022. *Adapting to Rising Flood Risk: An Analysis of Insurance Solutions for Canada.* Technical report. Public Safety Canada, Government of Canada, August.

Rhoades, Alan M, Andrew D Jones, Abhishekh Srivastava, Huanping Huang, Travis A O'Brien, Christina M Patricola, Paul A Ullrich, Michael Wehner, and Yang Zhou. 2020. The shifting scales of western us landfalling atmospheric rivers under climate change. *Geophysical Research Letters* 47 (17): e2020GL089096.

Ross, Brown, and Brasnett Bruce. 2010. *Canadian Meteorological Centre (CMC) Daily Snow Depth Analysis Data, Version 1.* Accessed August 3, 2021. https://doi.org/10.5067/W9FOYWH0EQZ3. http://nsidc.org/data/NSIDC-0447/versions/1.

Saerens, Marco, Patrice Latinne, and Christine Decaestecker. 2002. Adjusting the Outputs of a Classifier to New a Priori Probabilities: A Simple Procedure. *Neural Computation* 14, no. 1 (January): 21–41. ISSN: 08997667, accessed December 9, 2021. https://doi.org/10.1162/089976602753284446. https://search.ebscohost.com/login.aspx?direct=true&db=iih&AN=5672831&lang=fr&site=ehost-live.

Seirup, L, and G Yetman. 2006. U.s. census grids (summary file 1), 2000. *Palisades, NY: NASA Socioeconomic Data and Applications Center (SEDAC).*

Šeparović, Leo, Adelina Alexandru, René Laprise, Andrey Martynov, Laxmi Sushama, Katja Winger, Kossivi Tete, and Michel Valin. 2013. Present climate and climate change over north america as simulated by the fifth-generation canadian regional climate model. *Climate Dynamics* 41 (11-12): 3167–3201.

Surminski, Swenja, Laurens M Bouwer, and Joanne Linnerooth-Bayer. 2016. How insurance can support climate resilience. *Nature Climate Change* 6 (4): 333–334.

UN, (United Nations). 2023. *Disaster risk management, un-spider knowledge portal.* https://www.un-spider.org/risks-and-disasters/disaster-risk-management.

UNDRR. 2017. *Report of the open-ended intergovernmental expert working group on indicators and terminology relating to disaster risk reduction.* Technical report. United Nations Office for Disaster Risk Reduction, February.

Wood, S.N. 2017. *Generalized additive models: an introduction with r.* 2nd ed. Chapman / Hall/CRC.

Wright, Marvin N, S Wager, and P Probst. 2020. Ranger: a fast implementation of random forests. *R package version 0.12* 1.